

Influence of Electrode Corrugation after Calendering on the Geometry of Single Electrode Sheets in Battery Cell Production

Dominik Mayer,* Bastian Schwab, and Jürgen Fleischer

Calendering is an essential process step in battery cell production. By selective compaction of the material, the performance of the battery cell can be optimized. During processing, corrugations can occur in the machine direction, which are characterized in this article in relation to the material systems $\text{LiNi}_{0.8}\text{Mn}_{0.1}\text{Co}_{0.1}\text{O}_2$ (NMC811) and $\text{LiNi}_{0.6}\text{Mn}_{0.2}\text{Co}_{0.2}\text{O}_2$ (NMC622) as well as the rate of compaction and the web tension. It is shown that the corrugations are strongly dependent on the rate of compaction. The material system and the web tension show a weaker influence on the corrugation characteristics. Subsequently, single electrode sheets are cut from the coils and their geometry is investigated. It is shown that the corrugation hardly propagates further into the single electrodes, which is explained with the storage time of the electrodes. Rather, the coil bending strongly influences the electrode sheet geometry. It is shown that the position of the conductor tab also has an important influence.

1. Introduction

In the recent decade, the use of lithium-ion batteries has received an immense boost as they enable more sustainable mobility.^[1] Not only in the field of mobility but also in other applications such as grid storage and consumer electronics like powertools or e-bikes they are used.^[2] In the future, the market for lithium-ion batteries is expected to increase significantly.^[3] However, especially in the mobility sector, the costs for batteries are still high, which puts the focus on the associated battery cell production systems, as they are a key to low-cost and yet high-quality battery cells.^[4]

Especially for large-format and stacked or z-folded battery cells, it is a major challenge to produce precisely stacked cell

stacks with high quality and at the same time with high speed. An essential quality parameter here is the achieved stacking accuracy.^[5–7] An important influencing factor is the geometry of single electrode sheet (SES) from which the cell stack is formed. The literature shows that especially influences from previous calendering and separation have a significant impact on the geometry.^[8] In an influence analysis, Mayer and Fleischer show that the geometry of the SES can be influenced by the following factors:^[8] 1) electrode corrugation due to calendering process; 2) corrugation at the coating edge due to the coating and calendering processes; 3) bending of the whole electrode sheets due to coil bending after calendering and winding on coil; 4) length and width deviations of the sheet dimension due to calendering and singulation process; and 5) randomly distributed irregularities due to coating process and material irregularities.


A quantification of the individual influences is not carried out in this article. A first approach to investigate length and width deviations of SES is given by Weinmann et al.^[9] The dependence of the length and width dimensions on the applied web tension is investigated on a cut-and-place system developed by Baumeister and Fleischer and Baumeister.^[10,11]

So far, the most comprehensive investigation of the SES influence on stacking accuracy has been carried out by Weinmann.^[12] It is systematically analyzed that, in addition to the influence of the stacking machine and its parameter settings, the characteristics of the SES geometry have a significant impact on stacking accuracy.

A first approach for measuring the impact of corrugation after calendering on the geometry of SES is done by Mayer et al.^[13] It is described that the corrugation propagates into the SES depending on the rate of compaction. A high rate of compaction results in high deviations of the SES vertically to the contact surface. However, it is not clear how large the initial corrugations were after calendering in machine direction. This corrugation over the entire web width as well as smaller corrugations at the edge of the coating are described by both Bold and Fleischer and Günther et al.^[14,15]

Both publications show typical effects and defects that occur after calendering depending on the parameter set. Bold and Fleischer then focus on wrinkle formation, Günther et al. qualitatively evaluate the impact of the effects and defects after calendering on further processing in the subsequent processes, though a quantification does not take place.^[14,15] However, first

D. Mayer, B. Schwab, J. Fleischer
wbk Institute of Production Science
Karlsruhe Institute of Technology
Kaiserstraße 12, 76131 Karlsruhe, Germany
E-mail: dominik.mayer2@kit.edu

 The ORCID identification number(s) for the author(s) of this article can be found under <https://doi.org/10.1002/ente.202200870>.

© 2022 The Authors. Energy Technology published by Wiley-VCH GmbH. This is an open access article under the terms of the Creative Commons Attribution-NonCommercial-NoDerivs License, which permits use and distribution in any medium, provided the original work is properly cited, the use is non-commercial and no modifications or adaptations are made.

DOI: 10.1002/ente.202200870

quantification approaches are given by Mayr et al. for the corrugation in machine direction after calendaring.^[16] A laser triangulation line sensor is integrated into the calender, and the corrugation is recorded. Based on this, a defect evaluation index (DEI) is introduced. This is determined by the difference between the highest point of the corrugation amplitude and the lowest point. The application of the index is differentiated into the corrugations at the coating edge, to describe the edge corrugations, as well as the corrugation distributed over the width of the electrode. As an example for lithium and manganese-rich nickel–cobalt–manganese oxide (LMR-NCM) cathodes, the values for calendaring to about 30% porosity with calender rolls tempered to 23 °C are recorded. The edge corrugations show a DEI of 1.36 at the coating edge and the electrode corrugation a DEI of 3.22. Furthermore, the DEI of the edge corrugations is reduced by 9.6% when the roll temperature is increased to 90 °C and by 25.2% for the corrugations across the electrode width. A systematic investigation of the influences of different calendaring and material parameters is not carried out—the focus lies on the introduction of the sensor system.

The analysis of the literature shows that the impact of calendaring and especially the corrugation after calendaring on the geometry of the SES has hardly been systematically investigated. Weinmann analyzes the influence of SES geometry on stacking accuracy.^[12] However, the analysis is mostly done by a qualitative description of the causes without detailed parameter studies. It is not apparent to what extent the respective effects have an impact on the stacking accuracy. This influence can be investigated with simulation models, as Mayer and Fleischer points out, but requires information about geometric characteristics of SES.^[8] Therefore, in this article, the corrugations after calendaring and the resulting geometry of the SES will be systematically investigated and characterized. The investigations are carried out on the same basic electrode geometry as already presented in Mayer and Fleischer and Mayer et al.^[8,13] The novelty of the study can be summarized as follows. So far, the corrugations that can occur after calendaring have only been described qualitatively by Bold and Fleischer, Günther et al. as well as Mayr et al.^[14–16] Therefore, no study exists yet that quantitatively relates the corrugations after the calendaring process to the rate of compaction, the web tension, different active materials, and coating thicknesses. In addition, Weinmann has carried out mainly qualitative studies on the SES geometry, a quantitative investigation of the geometry has not yet been carried out in literature.^[12] Further, the influence of calendaring on subsequent processes was considered by Günther et al. within a determination of the defect influence on subsequent processes.^[15] However, a quantification between calendaring and SES geometry has also not yet been carried out in literature.

Consequently, this article is aimed to improve the understanding of the corrugations after calendaring as well as their effects on the geometry of the SES. With the aid of this knowledge, manufacturing tolerances for corrugations after the calendaring process and the SES can be defined more specific that helps to optimize the stacking process and its stacking accuracy.

2. Experimental Section

The two cathode active materials $\text{LiNi}_{0.8}\text{Mn}_{0.1}\text{Co}_{0.1}\text{O}_2$ (NMC811) and $\text{LiNi}_{0.6}\text{Mn}_{0.2}\text{Co}_{0.2}\text{O}_2$ (NMC622) were used for the experiments. Both materials were manufactured uncalendered with the same composition of 96% active material, 2% conductive additive, and 2% polyvinylidene fluoride binder (PVDF) by Enertech International and purchased by wbk Institute of Production Science. The electrodes were delivered uncalendered on coils that was necessary to conduct the calendaring experiments regarding the corrugations directly after the calendaring process. Loading densities of 41.6 and 55.0 g cm⁻² were used respectively. All materials were coated with a width of 155 mm on both sides, while the aluminum substrate foil had a total width of 215 mm and a thickness of 15 μm. Further material specifications can be found in **Table 1**.

The electrodes were first calendered, then the result was measured in the resting position in the tensioned state directly after the rollers stopped by using 3D scanning technology.

A calender of the GKL 500 MS series from Saueressig was used for the calendaring work. The rollers had a diameter of 700 mm and a width of 500 mm. Starting from the unwinding unit, the electrode material was guided via various deflection rollers to the main rolling mill, where it was calendered horizontally between the two main rollers. In the process, the main rollers were each at a 90° angle to the processed material, so that it can be further processed horizontally up to the resting position where the electrodes were scanned. The calendered electrode then ran via the tensioning unit, which supplied the required web tension, to the rewinder, where the calendered material was collected. They can be heated to a maximum of 90 °C and applied a maximum line load of 2000 N mm⁻¹. The line load was calculated from the resulting positioning forces for the rollers. To determine the layer thickness, a small piece of electrode was punched out using a mobile cutting pliers (EL-Cell GmbH, Hamburg, Germany). It was then measured with the tactile coating thickness device digital indicator MarCator 1075R (Mahr GmbH, Goettingen, Germany) and weighed with the laboratory balance EW 220-3NM (KERN & SOHN GmbH, Balingen-Frommern, Germany).

Table 1. Used materials and their specifications.

Material	Loading density both sides [mg cm ⁻²]	Electrode thickness [μm]	Coating density [g cm ⁻³]	Areal capacity [mAh cm ⁻²]	Particle-size distribution D50 (average particle size) [μm]	Particle-size distribution D90 [μm]
NMC811 (thin)	41.6 ± 0.5	204 ± 2	2.2	7.4	10	17.5
NMC811 (thick)	55.0 ± 0.5	260 ± 1	2.2	9.8	10	17.5
NMC622 (thin)	41.6 ± 0.5	191 ± 1	2.4	6.8	12	28.0
NMC622 (thick)	55.0 ± 0.5	242 ± 1	2.4	9.0	12	28.0

For the geometric measurement of the corrugation of the electrodes in the clamped state directly after calendaring, a 3D scanner of the ATOS Core 135 series from GOM (Carl Zeiss GOM Metrology GmbH, Braunschweig, Germany) was used. The device had a scanning field of about 135 mm × 100 mm with a camera resolution of 5 megapixels. For the measurement of larger components, individual images were superimposed by means of reference points which were applied to the electrode, so that in every scanning field, there were at least three known points from prior scans. These reference points were required by the GOM-Inspect software in order to transform partially captured point clouds of the electrode into a complete 3D object. In an industrial application, a laser triangulation sensor can be used to determine defect patterns in real time as described in Mayr et al.^[15] About 350 mm of the electrodes were used for evaluation. After the measurement, the electrodes were wound onto a coil with a diameter of 6 inches.

Further processing took place on the Coil2Stack machine, which was developed and set up at Karlsruhe Institute of Technology.^[17,18] The coils were clamped and separated into sheets of about 25 cm length using up to approx. 15 N web tension. Further processing of the electrode sheets followed Mayer et al.^[13] From the resulting sheets, the desired electrode sheets with the correct conductor shape were punched out by means of steel strip cutting. A laboratory steel strip cutting device from the company Manz was used for this purpose (Manz AG, Reutlingen, Germany). The resulting electrode dimension was about ≈200 mm × 135 mm.

The electrodes were then placed on a flat plate and geometrically measured using again the 3D scanner Atos Core 135 (Carl Zeiss GOM Metrology GmbH, Braunschweig, Germany). The entire experimental procedure is shown in **Figure 1**.

3. Results

The results are presented in a two-part structure. First, the corrugations of the electrodes are characterized depending on various calendaring and material parameters (3.1). Then the individual sheets separated from the calendared electrode coils are characterized (3.2).

3.1. Electrode Corrugation after Calendaring

3.1.1. Experimental Design

The presented materials NMC811 (thin), NMC811 (thick), NMC622 (thin), and NMC622 (thick) are used for calendaring. The temperature of the rollers is set to the possible maximum of 90 °C and kept constant throughout the tests. The reason for this is the knowledge from the literature that defect patterns are less pronounced at high temperatures due to the lower required line load and less mechanical stress that is induced into the material.^[16,19,20] Furthermore, the speed of the rollers is kept constant at 1 m min⁻¹.

The parameters varied in the tests are first the respective densities of the material. All materials were compacted in separate experimental series to about 15% and 25% of their original total thickness. In addition, the two NMC811 materials were compacted to 35% and the two NMC622 materials to 30% due to the maximum permissible line load of the calender. At the respective strongest compactions, 30% and 35%, the last deflection roller of the calender was skipped, as otherwise it would have led to tearing in the web.

Furthermore, the tests were varied with regard to the applied web tension in the three settings of 10, 30, and 50 N. A tabular overview of the test parameters can be found in **Table 2**.

By combining all the material and process parameters used, 36 series of experiments were carried out. In order to ensure the recognized correlations, e.g., of a linear or exponential nature in the investigated area, selected parameter configurations for NMC811 (thin) were measured in adjacent or intermediate

Table 2. Overview of applied experimental parameters.

	Parameter		
	Material	Rate of compaction [%]	Web tension [N]
Parameter values	NMC811 (thin)	15	10
	NMC811 (thick)	25	30
	NMC622 (thin)	30 (NMC622)	50
	NMC622 (thick)	35 (NMC811)	

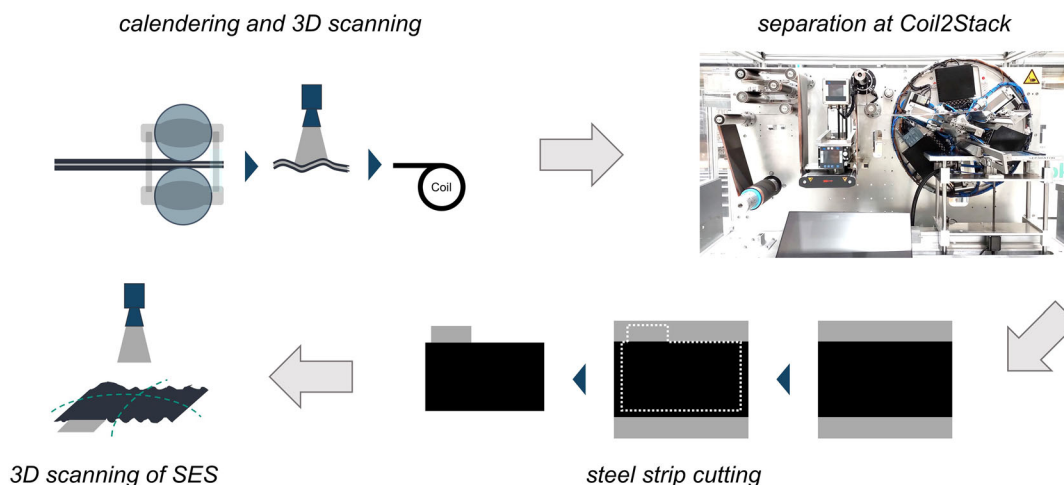


Figure 1. Visualization of the entire experimental setup. Adapted with permission.^[8] Copyright 2021, Elsevier.

parameter points in the sense of a sensitivity analysis. For this purpose, on the one hand, the stages 20% and 30% in combination with a constant web tension of 30 N were added for a more precise analysis of the influence of compaction. On the other hand, for the investigation of the web tension, the parameters 70 and 80 N in combination with the compaction level 25% complete the assurance of the correlations.

To evaluate the corrugation, a contour line was then drawn in the center of the web. Due to the very large number of data points, 36 representative values were taken at intervals of 10 mm along the contour lines, representing the curve in the respective area. Following Mayr et al., the DEI was then determined from the contour line.^[16] Figure 2 shows the measuring setup of an exemplary, corrugated electrode, which was calendered. The red 3D scanner is placed over the electrode and measures a part of the corrugated electrode surface. The measurement range is shown by the blue area. Several images are taken by the 3D scanner to cover the whole area of interest and stitched together to rebuild the surface. The virtually rebuilding of the surface is seen in the lower middle of Figure 2. In the middle of the coating area, the contour line is extracted by the GOM Inspect software, see the upper middle of Figure 2. On the right side, the DEI is determined by using the contour line.

3.1.2. Results and Discussion

First, the results for the investigation of the correlations between the corrugation or DEI and the rate of compaction as well as the web tension are shown, see Figure 3.

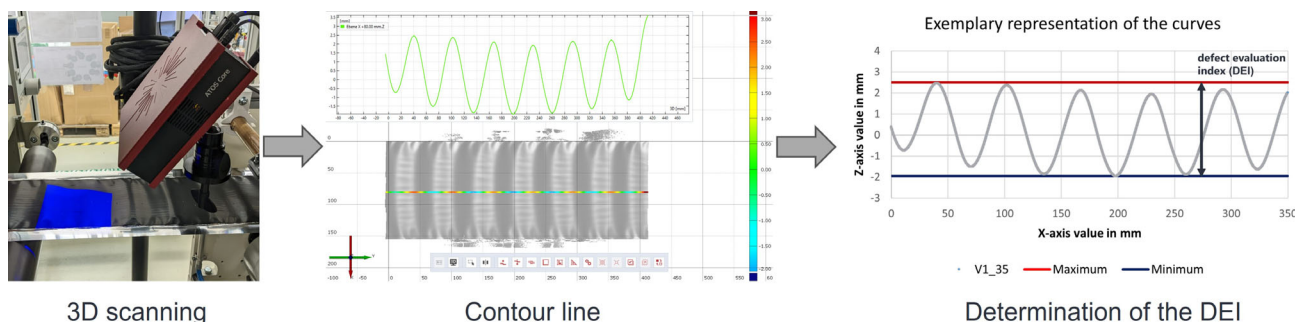


Figure 2. Measurement procedure for the electrode corrugation: scanning the calendered and corrugated electrode with 3D scanner (left) to get the contour line (middle) and calculating its DEI (right).

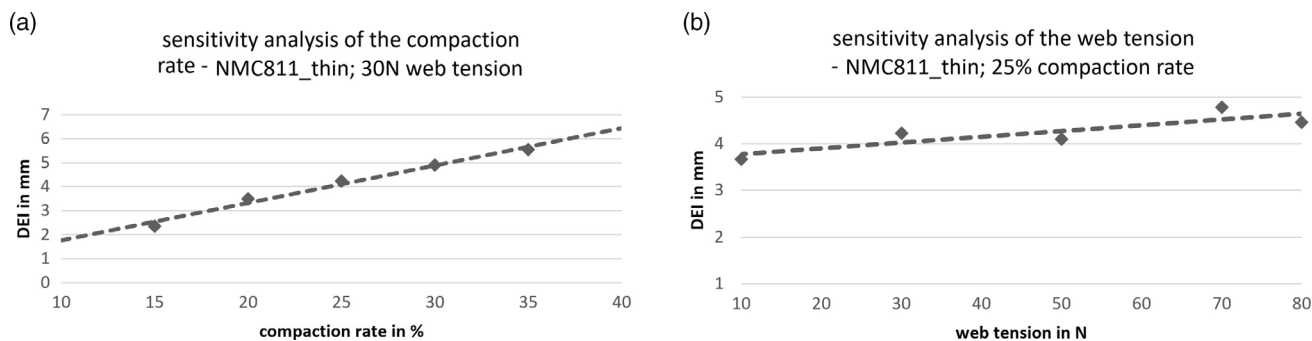


Figure 3. Sensitivity analysis of: a) compaction rate of NMC811 (thin) with compaction rates of 15%, 20%, 25%, 30%, and 35% and a constant web tension of 30 N, b) web tension of NMC811 (thin) with web tensions of 10, 30, 50, 70, and 80 N and a constant compaction rate of 25%.

All measurements were made of the same material (NMC811 (thin)) and have the same web tension of 30 N. It can be seen that NMC811 (thin) has a clear linear behavior in terms of DEI and densification in the considered range. The more the material is compressed, the greater the deformation and thus the corrugation in the center of the electrode. For the following tests, linear behavior can be assumed. Thus, in the following tests, only three compression levels per material are examined. For the web tension, the situation appears less clear. A slight linear increasing correlation can be recognized, which is, however, counteracted by a low coefficient of determination of 0.7285. However, the practical execution of the experiments shows that the processability of the electrodes decreases strongly at higher densities and higher web tension. For this reason, it was decided to pursue with 10, 30, and 50 N web tension for the following tests.

The results of the systematic parameter variation of web tension and rate of compaction are shown separated by material type in Figure 4.

As already assumed by Mayr et al., the DEI is a powerful representation to link the corrugations quantitatively with the compaction rate.^[15] Also the measured DEI are in the same range as they measured it. However, further comparisons cannot be made seriously, as the used electrode material is different. In the presented investigations, it can be seen that all materials show the behavior that a higher compression leads to a higher corrugation amplitude or DEI as shown here. This can be explained by the elongation of the coated material in the running direction compared to the uncoated substrate at the edge of the electrode. The uncoated areas retain their original length due to the lack of contact with

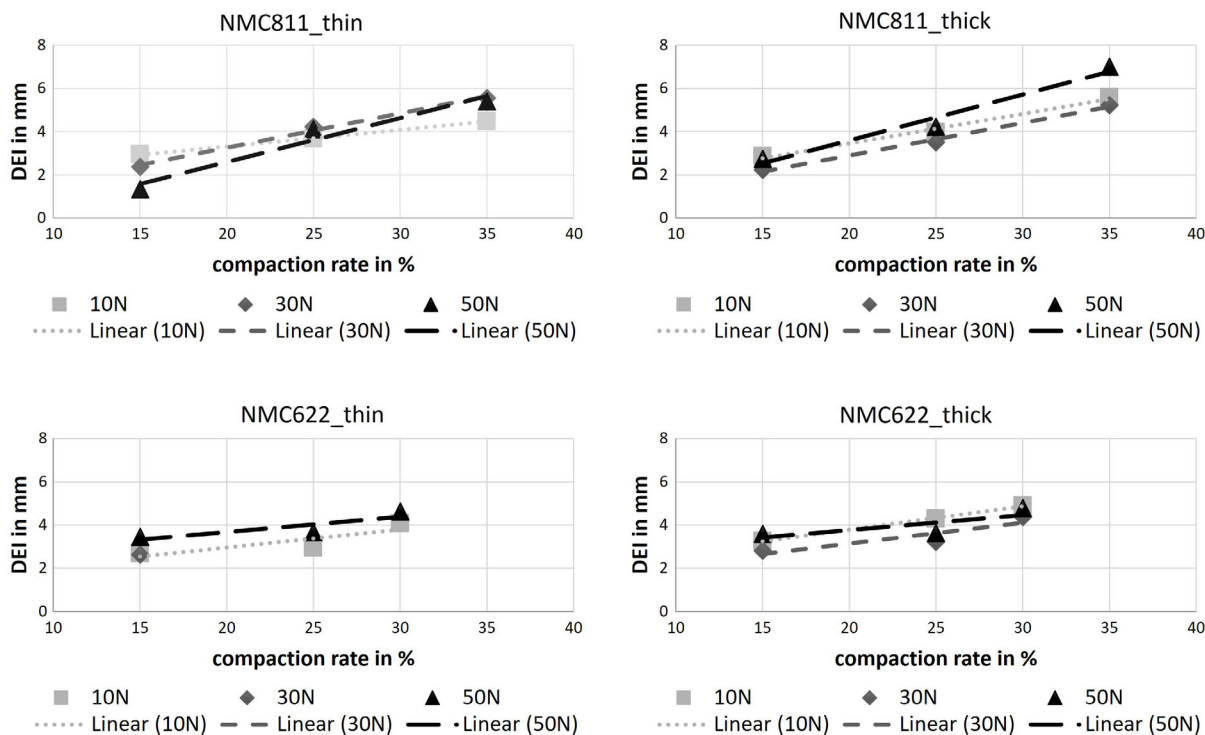


Figure 4. Results of DEI for all parameter variations (compaction rates: 15%, 25%, 30%, or 35%; web tension: 10, 30, and 50 N) and different materials (NMC811 (thin), NMC811 (thick), NMC622 (thin), and NMC622 (thick)). Additional linear lines for the trend of compaction rates, determined through linear regression.

the rollers, the coated area experiences an elongation in and vertical to the machine running direction due to the compression, which is also mentioned by Bold and Fleischer.^[13] The elongation in the running direction, which depends on the rate of compression, then provides the corrugation formation. Furthermore, it can be seen that the same percentage of material compression also leads to similar corrugation amplitudes, which supports the explanation above. However, no systematic difference between the different materials can be detected nor can a connection between the web tension and the DEI be identified. Based on the findings of Mayr et al., it can be assumed that the corrugations can still be influenced by the preheating of electrodes or a higher temperature of the rollers.^[15] It can be assumed that at

higher temperatures, less stress is introduced into the material due to the softer binder condition. This allows to expect less corrugations. In any case, this must be investigated in further studies.

For further evaluation of the investigations, the number of amplitudes is counted in a fixed range of 300 mm, averaged over the different rates of compaction and plotted over the web tension according to the material in order to obtain an indication of the corrugation frequency. The results are shown for NMC811 in Figure 5a and for NMC622 in b.

It can be detected that the number of amplitudes tends to fall as the web tension increases. This indicates that the web tension does not influence the amplitude of the corrugations, but the

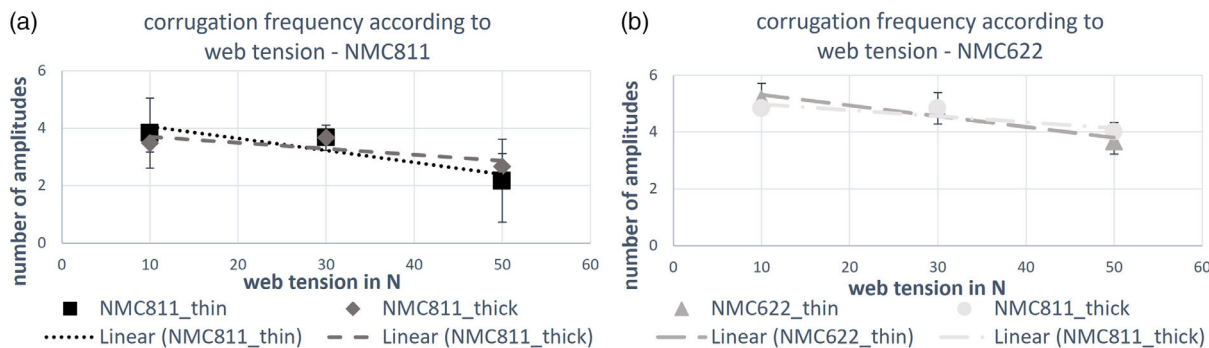


Figure 5. Corrugation frequency according to web tension for a) NMC811 and b) NMC622.

length becomes longer. There is hardly any difference between the thin and thick coating in both cases. However, the materials differ significantly from each other: NMC622 has a significantly higher corrugation frequency than NMC811. This can be explained by the increased line loads of the NMC622 material, which had no influence in the evaluation of the DEI, but are noticeable here by an increased corrugation frequency. The higher line loads for the NMC622 material can be observed in **Table 3**. This phenomenon has also already been described of Meyer and can be explained through a higher compaction resistance of the NMC622 material in comparison to NMC811.^[21] An explanation for the higher compaction resistance could be the particle size. As listed in Table 1, the particle size of the two active materials differs. Compaction causes individual particles to be displaced and arranged differently, the ideal state here would theoretically be the close packing of equal spheres. It can be assumed that in general smaller spheres can slide along each other more easily and therefore the forces for this and thus the resulting compaction resistance is smaller.

3.2. Characterization of Single Electrode Sheets

3.2.1. Experimental Design

After calendaring, the electrodes are wound onto coils with a 6 inch diameter via several deflection rollers. In the test series with

Table 3. Applied line loads for compaction rates in different materials.

Material	Rate of compaction [%]			
	15	25	30	35
NMC811 (thin)	280 ± 15	540 ± 12	–	1550 ± 20
NMC811 (thick)	300 ± 12	640 ± 14	–	1850 ± 35
NMC622 (thin)	360 ± 8	780 ± 12	1370 ± 19	–
NMC622 (thick)	380 ± 18	860 ± 10	1850 ± 22	–

the highest densities, 30% for NMC622 and 35% for NMC811, the last deflection roller was skipped during the winding process on the calender, as otherwise further processing would not have been possible due to foil tearing. The electrodes were then further processed on the Coil2Stack machine. Also the electrodes with 30%, respectively, 35% compaction rate could not be processed, and instead had to be separated manually. It can be confirmed that automated further processing of highly compacted electrodes leads to problems in laboratory battery pilot lines, as also mentioned in the literature.^[15,16] However, it cannot be excluded that measures such as parameter fine tuning or specialized process adaptations, such as deflection rollers with larger diameters, are carried out on the industry side, so that the strong densifications are nevertheless investigated further as a worst case. In addition, trends can be better identified in this way.

After separation with the Coil2Stack machine, the sheets are separated by steel strip cutting, placed on a flat plate and measured using a 3D scanner. Depending on the amount of material available, 5 to 10 electrode sheets were measured. In total, 325 SES were measured for data acquisition. It turned out that the resulting electrode geometry changes significantly depending on the pick-up side, i.e., the imaginary coil core lies above or below the electrode, which was already described in literature.^[13] To investigate the effect, two measurements (side A with imaginary coil core is above and side B with imaginary coil core is below) were made for each electrode sheet. To quantify the geometry, height contours were again drawn at interested points on the SES. Details are shown in **Figure 6**.

3.2.2. Results and Discussion

First, three contour lines (10, 70 and 130 mm, see Figure 6) of an exemplary SES are evaluated on both sides and shown in **Figure 7**. Care was taken to select an SES that represents the most SES qualitatively.

The evaluation of side A shows that all the height profiles shown have an upward curvature. It shows that the winding process on the

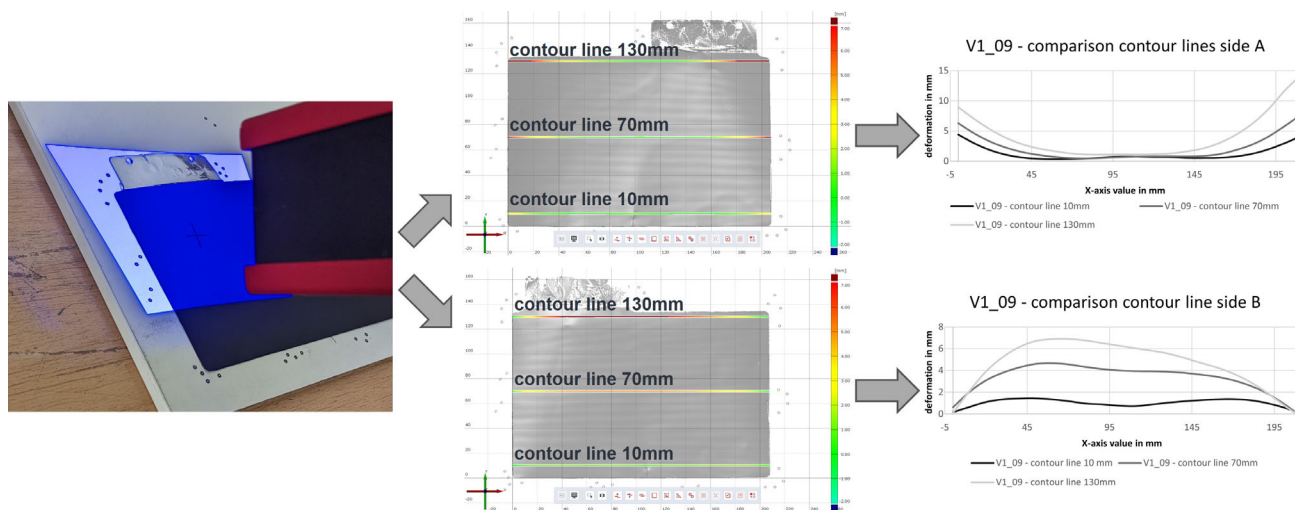


Figure 6. 3D scanning, measuring, and determination of the maximum deformation in SES.

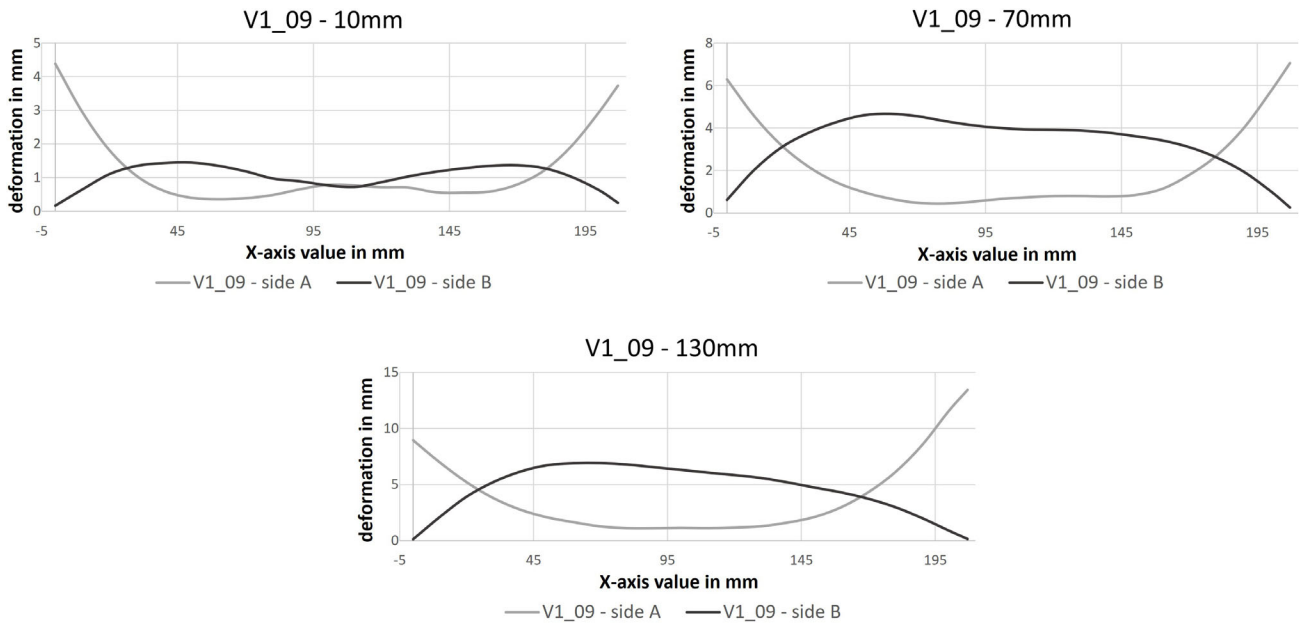


Figure 7. Contour lines 10, 70, and 130 mm for both pick up sides.

electrode coil and thus the radius of the coil has an important influence on the later SES geometry. In case of side B, it can be seen that the imaginary core of the coil lies below the diagram.

Furthermore, the observation of side A shows that values of the contour lines increase from profile 10 mm to profile 130 mm, and that the global maximum of a sheet (in contour line 130 mm) is located at the right edge and thus next to the conductor tab of the SES in all test series and is strongly pronounced. On side B, this is exactly the opposite, and it can be seen that the maximum is more to the middle left, and thus also on the side of the conductor tab. These two observations can be explained by the significant influence of the conductor tab that prevents the coating from expanding after cutting. The tendency of the maximum to occur close to the conductor tab is also reflected in the distribution of the position of all maxima in **Figure 8a, b**. For this purpose, representative values were taken along the contour line 130 mm of all evaluated SES per parameter setting and averaged arithmetically, whereby a characteristic contour line 130 mm per parameter setting was formed in each case. From these characteristic contour lines, the maximum was identified and its X-axis value determined. Subsequently, a

distribution of the maxima of all 40 test series considered was created for sides A and B.

Surprisingly, the described corrugation in the calendaring process is hardly transferred to the SES—in contrast to what is described in Mayer et al., where a clear pronouncement of the corrugation could be recognized.^[13] The coil winding after calendaring initially pushes the corrugations outward and winds the coil smoothly. To explain the difference to literature, it is assumed that the duration of the electrode coil storage time has a decisive influence on the expression of the corrugation in the SES. Sangrós et al. speak of a visco-elastic material behavior of the electrode coating, which is therefore time dependent.^[22] The longer the coil material is stored, the more it takes on the form of coil bending due to the visco-elastic material behavior, so that coil bending becomes the dominant factor after a longer period of time. In this article, the coils were stored in an argon atmosphere for several weeks after calendaring due to laboratory availability. The specified times of storage are mentioned in **Table 4**. No time is mentioned in Mayer et al.^[13]

For further investigation, the profile contours of all individual SES of the previously calendared electrodes are evaluated. For

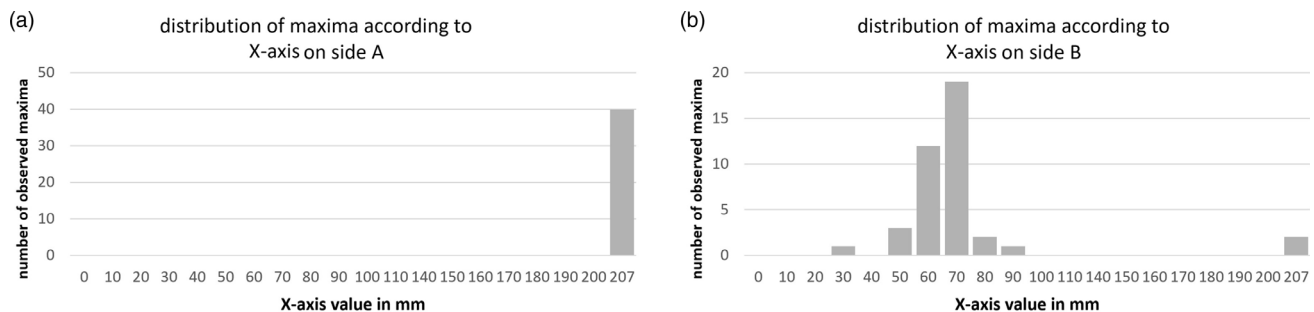


Figure 8. Distribution of maxima on: a) side A and b) side B.

Table 4. Storage time between calendering and separation to SES.

Material	Rate of compaction [%]			
	15	25	30	35
NMC811 (thin)	5	5	–	2
NMC811 (thick)	10	10	–	10
NMC622 (thin)	5	5	5	–
NMC622 (thick)	7	7	6	–

this purpose, analogous to the methodology in Section 3.1.2, the profile contour in the middle of the SES is considered (see contour line 70 mm in Figure 6), and the respective maximum is identified and averaged over the number of measured SES. The focus is on the B-side. **Figure 9** shows the result of the evaluation. Each data point consists of 5 to 10 evaluated SES profile contours.

It can be seen throughout that greater compaction leads to higher expression of the contour line. It can be assumed that the greater compaction leads to a stronger stiffening of the material. This leads to a higher resistance of the SES against the weight force and thus against lowering onto the flat table plate. The influence of the web tension during calendering has no discernible effect on the maximum.

For a more detailed observation and discussion of the SES regarding the compaction rate, the contour line 70 mm of the B-side and the test series with 10 N web tension are selected, see **Figure 10**. Due to the large number of data points, representative values were taken every 10 mm on the contour line at the same point on the longitudinal axis/X-axis and these were then arithmetically averaged per each material.

Again, the curve progression of the contour line depending on the rate of compaction is initially evident across all materials. However, when comparing the materials, it is noticeable that the contour lines of NMC811 (thin) are clearly below those of NMC622 (thin) and of NMC811 (thick) below those of NMC622 (thick), although the same surface loading and the same or similar compaction rate are the basis in each case.

It can therefore be concluded that the calendering process inserts a higher stiffness in the NMC622 electrodes, which also influences the geometry of the SES. A higher compaction resistance of NMC622 can be assumed in relation to NMC811 and which can also be proven by the measured line loads during calendering of the electrodes in Table 3. Also, the initial, uncalendered density of NMC622 is higher than NMC811 since the loading density is the same but the coating thickness of NMC622 is lower, see Table 1.

Regarding the loading density, NMC811 shows that the thinner coating has a lower height in the contour line and thus a lower resistance against flattening can be assumed. This can be explained by the fact that despite of the lower coating thickness, the same rate of calendering and therefore the same stiffness properties of the coating exist in principle, but there is significantly less material that opposes the weight force and therefore the thicker coating has a higher contour line in absolute terms.

In NMC622, the effect is not seen, on the contrary, the contour lines of the thin and the thick coating are very similar to each other as well as in total higher than the NMC811 contour lines. First, it can be concluded that in general NMC622 is stiffer than NMC811 because of the higher line load. To explain the similar contour lines between both NMC622 materials, it is assumed that the ratio between stiffness and weight per cm² seems equivalent in contrast to NMC811.

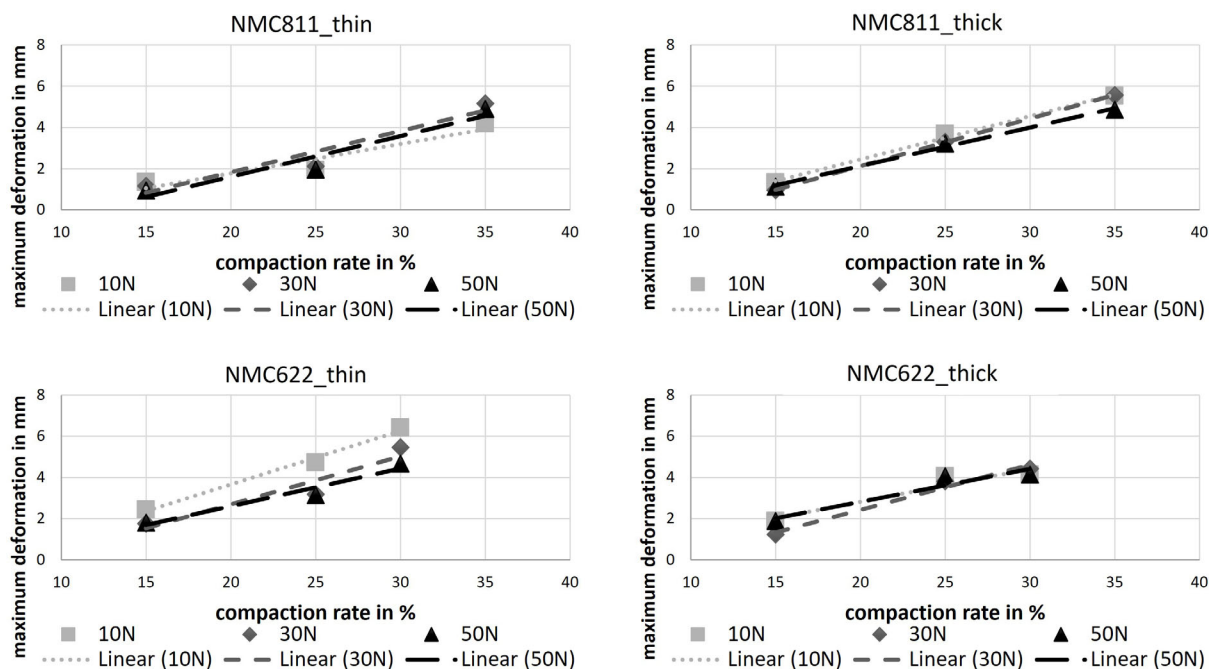


Figure 9. Results of maximum deviation in SES for all parameter variations and different materials.

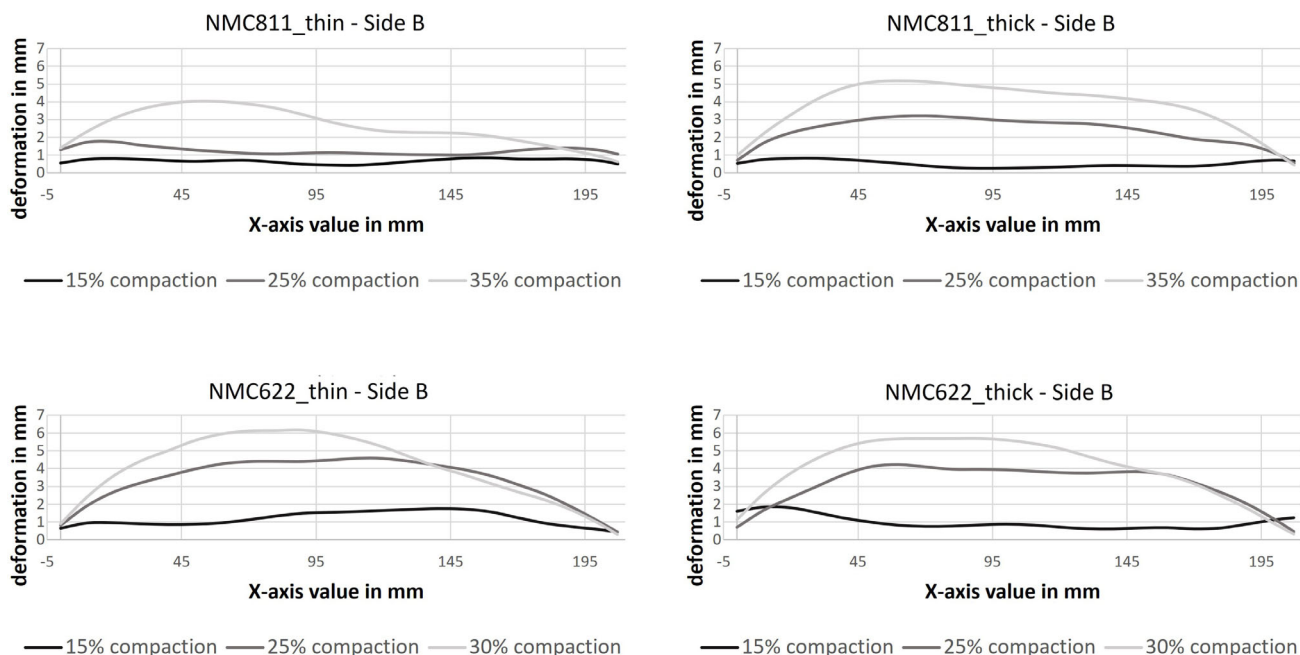


Figure 10. Comparison of compaction rates in different materials for contour line 70 mm.

4. Summary and Outlook

In this article, the corrugation of the electrodes after calendaring was investigated first. For this purpose, the electrodes were geometrically measured after calendaring and evaluated by means of DEI. It was found that the DEI increases linearly with the degree of compaction. The material and the web tension have only a minor influence.

Subsequently, SES was cut from the electrodes, and the resulting geometry was examined. The remaining coil bending in the SES has a significant influence on the resulting geometry. The conductor tabs also have a decisive influence on the geometry.

The investigations lead to the conclusion that the storage time of the coil after calendaring has an important influence on the resulting SES geometry. Further investigations are needed to identify this relationship in detail. Based on the geometry of the SES, the further processability is crucial. In further studies, it must be investigated the influence the resulting geometries have on the following process steps. Particularly in the stacking process, a large influence of the geometry is to be expected with regard to the stacking accuracy that can be achieved. These relationships must be investigated in further studies in order to be able to finally define tolerances for the corrugations after calendaring regarding the subsequent production process steps.

Acknowledgements

This work was funded by the German Federal Ministry of Education and Research (BMBF) within the Project "Sim4Pro" (grant number 03XP0242C) and was done at the KIT Battery Technology Center (KIT-BATEC) and contributes to the research performed at CELEST (Center for Electrochemical Energy Storage Ulm-Karlsruhe). In addition, the

authors would like to thank Jonathan Bernecker for his support throughout the calendaring of the electrodes for this article.

Open Access funding enabled and organized by Projekt DEAL.

Conflict of Interest

The authors declare no conflict of interest.

Data Availability Statement

The data that support the findings of this study are available from the corresponding author upon reasonable request.

Keywords

battery cell manufacturing, calendaring, geometric effects, single electrode sheets, singulation

Received: August 1, 2022

Revised: November 8, 2022

Published online:

- [1] International Energy Agency (IEA), Global EV Outlook 2022. Securing Supplies for an Electric Future, <https://www.iea.org/reports/global-ev-outlook-2022> (accessed: July 2022).
- [2] M. Li, J. Lu, Z. Chen, K. Amine, *Adv. Mater.* **2018**, *30*, 1800561.
- [3] Y. Zhao, O. Pohl, A. I. Bhatt, G. E. Collis, P. J. Mahon, T. R ther, A. F. Hollenkamp, *Sustainable Chem.* **2021**, *2*, 167.
- [4] F. Duffner, L. Mauler, M. Wentker, J. Leker, M. Winter, *Int. J. Prod. Econ.* **2021**, *232*, 107982.
- [5] A. Kwade, W. Haselrieder, R. Leithoff, A. Modlinger, F. Dietrich, K. Droeder, *Nat. Energy* **2018**, *3*, 290.

- [6] R. Leithoff, A. Fröhlich, K. Dröder, *Energy Technol.* **2020**, *8*, 1900129.
- [7] G. Bach, *Dissertation*, Technische Universität Berlin, Berlin **2016**.
- [8] D. Mayer, J. Fleischer, *Procedia CIRP* **2021**, *104*, 744.
- [9] H. W. Weinmann, F. Lang, J. Hofmann, J. Fleischer, *wt Werkstattstechnik online* **2018**, *108*, 519.
- [10] M. Baumeister, J. Fleischer, *CIRP Ann.* **2014**, *63*, 5.
- [11] M. Baumeister, *Dissertation*, Karlsruher Institut für Technologie, Karlsruhe **2017**.
- [12] H. W. Weinmann, *Dissertation*, Karlsruher Institut für Technologie, Karlsruhe **2022**.
- [13] D. Mayer, A.-K. Wurba, B. Bold, J. Bernecker, A. Smith, J. Fleischer, *Processes* **2021**, *9*, 2009.
- [14] B. Bold, J. Fleischer, *Z. wirtsch. Fabrikbetr.* **2018**, *113*, 571.
- [15] T. Günther, D. Schreiner, A. Metkar, C. Meyer, A. Kwade, G. Reinhart, *Energy Technol.* **2020**, *8*, 1900026.
- [16] A. Mayr, D. Schreiner, B. Stumper, R. Daub, *Procedia CIRP* **2022**, *107*, 295.
- [17] H. W. Weinmann, H.-C. Töpfer, J. Fleischer, *Z. wirtsch. Fabrikbetr.* **2020**, *115*, 241.
- [18] H. W. Weinmann, M. Eichelkraut, L. Da Woke Silva, J. Fleischer, *C2 Coat. Converting* **2020**, *4*, 21.
- [19] C. Meyer, M. Weyhe, W. Haselrieder, A. Kwade, *Energy Technol.* **2020**, *8*, 1900175.
- [20] D. Schreiner, T. Zünd, F. J. Günter, L. Kraft, B. Stumper, F. Linsenmann, M. Schüßler, R. Wilhelm, A. Jossen, G. Reinhart, H. A. Ga, steiger, *J. Electrochem. Soc.* **2021**, *168*, 30507.
- [21] C. Meyer, *Dissertation*, Technische Universität Braunschweig, Braunschweig **2019**.
- [22] C. Sangrós Giménez, B. Finke, C. Schilde, L. Froböse, A. Kwade, *Powder Technol.* **2019**, *349*, 1.